UMass-Lowell Results of the IAEA Benchmark Calculation of Radioactive Inventory for Fission Reactor Decommissioning

Dr. John R. White and Mr. Andrew P. Fyfe

Chemical and Nuclear Engineering Department
University of Massachusetts-Lowell
Lowell, Massachusetts 01854

July 7, 1995

Prepared as part of an IAEA Benchmark Exercise

for the

International Atomic Energy Agency, Vienna, Austria

UMass-Lowell Results of the IAEA Benchmark Calculation of Radioactive Inventory for Fission Reactor Decommissioning

Dr. John R. White and Mr. Andrew P. Fyfe
Chemical and Nuclear Engineering Department
University of Massachusetts-Lowell, Lowell, Massachusetts 01854

July 7, 1995

Introduction/Overview

In January 1994, the University of Massachusetts Lowell (UMass-Lowell) was invited by the International Atomic Energy Agency (IAEA) to participate in an international benchmark exercise to address the adequacy of current cross section data and computational methods for quantifying neutron activation in the excore regions of commercial power reactors.[1] The ability to accurately predict the inventory of several relatively long-lived radioactive isotopes that result from years of exposure to a neutron environment is of critical concern for planning and executing a rational, safe, and economical decommissioning strategy.

The central focus of the benchmark exercise involved comparison of calculated results to measured activation data from the Japan Power Demonstration Reactor (JPDR).[2] The available experimental data include radial and axial activity profiles at various locations in the excore structure and bioshield materials for several important radioactive isotopes (^{60}Co, ^{54}Mn, ^{55}Fe, etc.). The benchmark exercise required the development of detailed computational models of the JPDR based on the geometry, material, and operational data supplied in Refs. 2 and 3, and the calculation of the space and energy dependent neutron flux throughout the model (using discrete ordinates transport theory). The induced activities at several desired locations were then computed with a newly-developed space-energy activation analysis code called ACTIV. This code uses the power history of the JPDR to normalize the pointwise multigroup neutron fluxes from the transport calculations to compute the time-dependent inventory of the important activation products in any desired location outside the active core region. ACTIV uses an ENDF/B-VI multigroup activation cross section library that is fully compatible with the group structure used within the transport calculations. The results from the ACTIV code were then compared to measured activation data from the JPDR decommissioning program.

The purpose of this report is to document the UMass-Lowell results for the JPDR activation analysis benchmark. The report first documents the data and methods incorporated within the actual codes utilized in the analysis, highlighting, of course, the new ACTIV code and its integration within an existing code system for performing excore and ex-vessel transport theory computations.[4] The details of our specific RZ geometric models of the JPDR configuration within the context of the DORT discrete ordinates transport code[5] are also reviewed, as well as the development of the absolute

normalization of the neutron source distribution used to drive the DORT fixed-source computations.

Important neutron flux data from the DORT analyses are summarized into three groups (fast, epi-thermal, and thermal) for efficient presentation of these data. However, the full multigroup fluxes (47 groups for the DORT 2-D analyses) were utilized with a compatible activation cross section library within ACTIV to produce activities for several key isotopes. The computed activities are compared directly with the JPDR measured data given in Ref. 2. These calculated-to-experimental comparisons are made at various radial and axial locations within the excore regions of the JPDR, and they show relatively good agreement for all the measured isotopes out through the pressure vessel region. Some significant discrepancies, however, are observed at relatively large distances within the concrete bioshield.

Preliminary results from this benchmark exercise were reviewed at an IAEA Consultant's Meeting in December 1994. All participants had roughly similar results, especially with the generally poor agreement between measured and computed activities in the bioshield region. Several questions were raised concerning the simplified bioshield geometry data given in Ref. 2, and subsequent correspondence[3] has identified additional geometry details, including the location and number of cooling tubes and rebar structural reinforcements within the bioshield region.

Based on data from Ref. 3, a new bioshield model was constructed and the results from this model (which is referred to as the Case B model) are given here as the best UMass-Lowell results to date for the JPDR activation benchmark. Some comparisons to the results from the original model (referred to as the Case A model), which was based entirely on Ref. 2, are also included to highlight the improvement obtained with the more detailed bioshield representation. However, although significant improvements were achieved, some large discrepancies are still apparent within the concrete bioshield.

Several sensitivity studies have been initiated in a continuing attempt to resolve the bioshield discrepancies. At present, it appears that much of the observed error may be due to poor energy detail at low energies in the current computations. Some 1-D fine group calculations (with several thermal groups) have been performed and they suggest that the 47-group BUGLE-93 library[6] is simply not adequate for accurately determining the thermal flux in the vessel-cavity-bioshield regions. Preliminary results from this work are briefly summarized at the end of this report, with a focus on the future work that is clearly needed to resolve this issue.

Data, Methods, and Codes

The nuclear data needed for neutron activation studies fall into two general categories:

1. multigroup neutron cross sections for use in the transport calculations to compute the space and energy dependence of the neutron flux, and

2. multigroup activation cross sections (n,γ, n,p, n,2n, etc.) and decay data (natural abundances, halflifes, branching fractions, etc.) for all the important parent and daughter isotopes that can be generated via neutron activation.

If possible, the transport calculation and the activation analysis should be done with a consistent set of multigroup data. However, in practice, the two calculations are often done independently and are only loosely connected via a set of collapsed neutron flux information from the transport calculation that is used in zero-dimensional few-group codes that model and simulate the isotope transmutation schemes. Usually significant detail is lost in this space and energy collapsing process, which can lead to large uncertainties in the computed activities. This is especially true in regions where rapid changes in the neutron spectra cannot be treated adequately in a zero-dimensional model. In addition, the coupling process is often somewhat cumbersome, since it usually requires a fair amount of manual intervention.

The new ACTIV code, which was developed recently at UMass-Lowell, eliminates this separate coupling and collapsing process by simply performing the activation calculations with the full space and energy dependent fluxes from the transport code. The same geometry is modeled and the user can select any number of pointwise radial and axial traverses or zone average activations that he or she desires. Thus, all of the space-energy detail from the original transport calculation is preserved and included within the activation calculation – thereby, essentially removing all the uncertainty that is introduced in the traditional two-step process. Now, the only uncertainties remaining are those associated with the computed neutron fluxes, the base activation data used within the ACTIV code, and, of course, the initial impurity concentrations present in the unirradiated structural materials.

The UMass-Lowell JPDR benchmark computations used the DORT code[5] for the transport calculations and the ACTIV code for the activity computations. The BUGLE-93 library[6] was used for all the 2-D transport calculations within DORT. The BUGLE-93 data include information for 120 isotopes/materials in 47 neutron groups and 20 gamma groups. This broad-group data set was collapsed from the VITAMIN-B6 fine-group library which contains 199 neutron group and 42 gamma group information derived from the ENDF/B-VI nuclear data files.[6] The BUGLE-93 library was designed specifically for shielding applications focusing on fast neutron and gamma transport analyses, vessel damage studies, excore dosimetry evaluations, etc., and it is not considered a very reliable data base for determining thermal fluxes, thermal reaction rates, and thermal neutron activation – since there are only two energy groups below 0.4 eV. However it has several positive attributes including the fact that it contains the latest ENDF data, it is readily available to the user community, and it already has a wide user base. In addition, the generation of a new multigroup library, that includes all the features of BUGLE-93 with greater thermal energy detail, was well beyond the scope of work for performing this benchmark analysis. Thus, it was decided that BUGLE-93 would be used exclusively for the 2-D DORT computations – and that the results of this exercise would be a good test of the utility of the BUGLE-93 library for general activation studies.

For full consistency, the activation cross sections used within ACTIV were also derived from VITAMIN-B6. The 199-group neutron data from the fine-group library were

collapsed to the BUGLE-93 47-group structure using the same concrete weighting spectrum utilized in the generation of BUGLE-93 from VITAMIN-B6. Eight separate reaction cross sections were extracted from the collapsed library and stored in a format suitable for use in ACTIV. The specific reactions and the associated ENDF MT numbers that are included in the ACTIV activation library are listed below:

ENDF MT No.	102	107	103	16	104	105	18	27
Reaction	n,γ	n,α	n,p	n,2n	n,d	n,t	n,f	n,abs

For the activation calculations, in addition to the neutron cross sections, natural isotopic abundances, decay data, and appropriate branching fractions are also needed. These data were obtained from the ENDF/B-VI version of the ORIGEN data libraries that are distributed as part of the SCALE 4.2 package.[7] The necessary data were extracted from the ORIGEN data files and incorporated into the activation library used within ACTIV.

The final activation library, called VB6ACTXS.LIB, has all the required nuclear data for subsequent activation analyses within ACTIV. This library contains base information for approximately 800 isotopes (nuclides from the ORIGEN data files), but it only has activity cross sections for about 100 isotopes (nuclides from the VITAMIN-B6 library). However, as new cross section information for additional isotopes becomes available (in the VITAMIN-B6 master library format), it can be incorporated within VB6ACTXS.LIB quite easily.

A simplified schematic that illustrates the development of the activation library used within ACTIV is shown in Fig. 1. This figure summarizes the various steps involved in the generation of VB6ACTXS.LIB. Most of the codes mentioned (MALOCS, NITAWL-II, ALPO, and ORIGEN) are part of the SCALE 4.2 package.[7] ACTXS, the last code in the sequence, was written at UMass-Lowell to integrate all the necessary nuclear data into a single file, VB6ACTXS.LIB, for use in ACTIV.

The ACTIV code itself uses the traditional matrix exponential technique for solution of the nuclide transmutation equations. The primary computational algorithms for the matrix exponential method were taken from the DEPTH-CHARGE modules of the VENTURE code system.[8-9] The ACTIV code simply reads the appropriate nuclide chain information, geometry data, initial isotope densities, and operational power versus time data and, using the precomputed space-energy fluxes from DORT and the nuclear data from VB6ACTXS.LIB, computes the time-dependent isotope inventories for each spatial point or zone of interest. The data flow and interaction between DORT and ACTIV are illustrated in Fig. 2. The summary edit from ACTIV gives the activity in Bq/g for the desired isotopes, spatial locations, and time points. These data can then be plotted or tabulated for further analyses – which, in the present JPDR benchmark study, involves direct comparison to the measured data from Ref. 2.

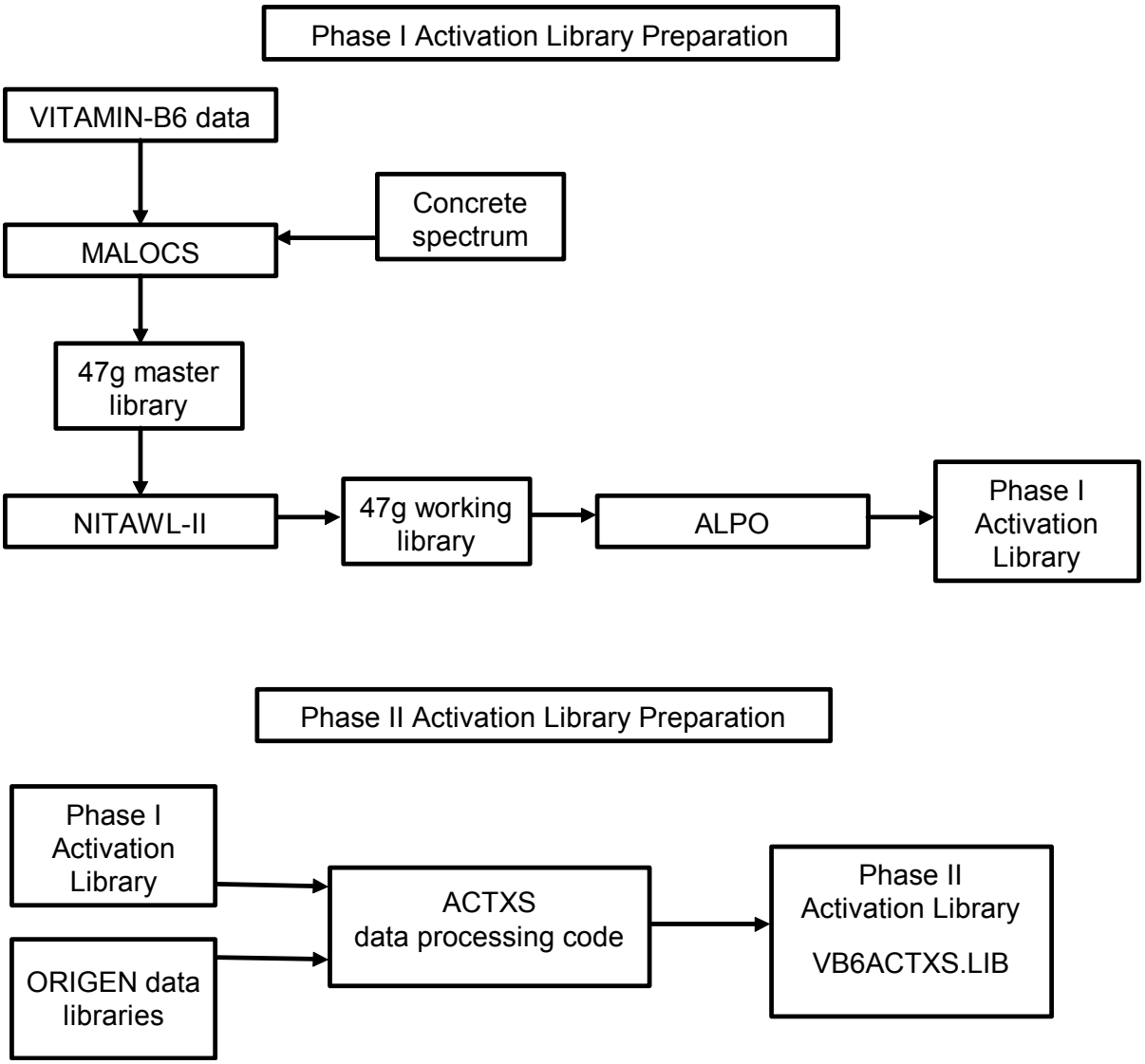

Fig. 1. Simplified schematic showing the development of VB6ACTXS.LIB.

JPDR Modeling Within DORT

The bulk of the effort needed for performing the JPDR benchmark analyses was related to the development and execution of the DORT models that were used to compute the space-energy distribution of the flux throughout the system. The Japan Power Demonstration Reactor (JPDR) was a direct-cycle BWR with dimensions that spanned over 12 m axially and 4 m radially. The reactor operated intermittently with varying power level over a period of about 13 years, from 1963 to 1976, with a total reactor thermal output of 21,500 MWD.

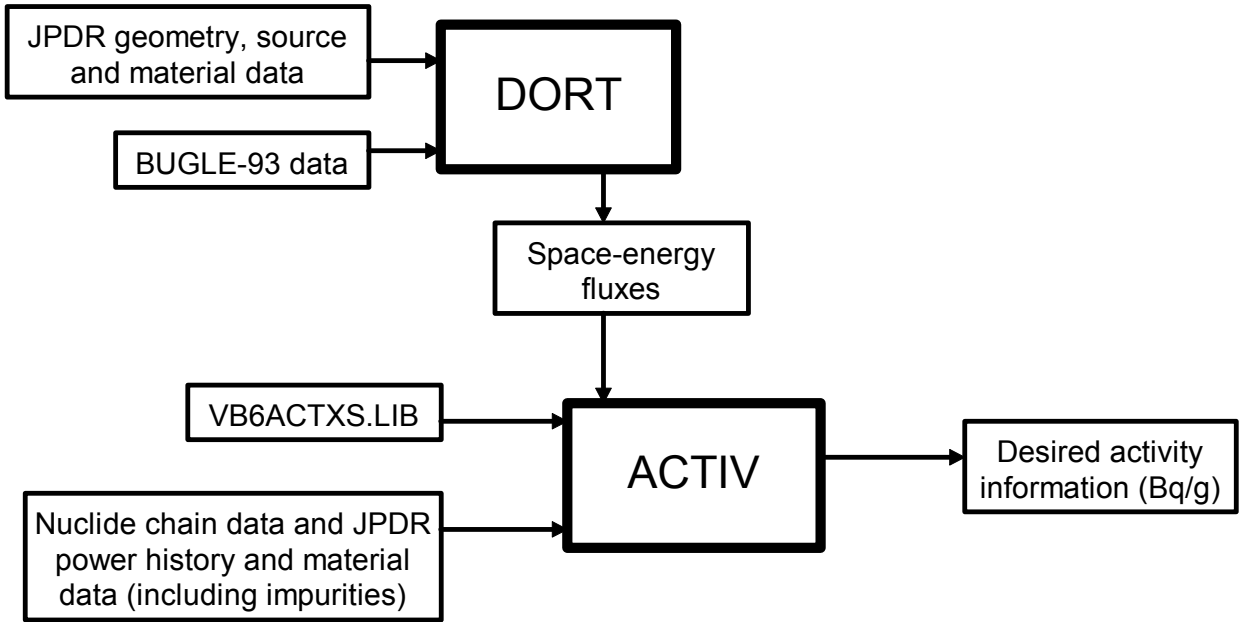

Fig. 2. Data flow and interaction between DORT and ACTIV.

After making a series of drawings of the reactor based on data from Ref. 2, it was apparent that the overall computational model would have to be broken into multiple sections axially, since a single DORT calculation with sufficient detail would be totally impractical. Therefore, the 12.2 m axial dimension was broken into three regions and labeled accordingly, with Region 1 at the bottom and Region 3 at the top. A bootstrapping technique, which couples one axial region to another via a saved internal boundary source is envisioned as a mechanism to complete the full benchmark computation.

An overall radial dimension of 3 m was used in the DORT models, with the radial fine mesh layout remaining the same in each axial model so as to maintain spatial continuity from one axial region to the next. This continuity is required for proper alignment of the saved boundary sources that couple the axial models. The axial locations of the saved boundary sources are in relatively homogeneous regions well above and below the active core zones. These locations seem very reasonable, since they allow regions of practical size to be modeled while, at the same time, placing the boundary sources in regions relatively far away from structural materials where backscatter may be important.

Modeling of the JPDR started at Region 2 which contains the core, and hence, the neutron source which drives the entire model. This is the only computation that has been completed at present. However, internal sources were saved at an axial distance of about 100 cm from the top and bottom boundaries of the model. These sources can be used to continue computations into the upper and lower structural regions of the JPDR configuration, if desired.

The Region 2 RZ geometric models in DORT spanned a radial distance of 300 cm and an axial dimension of about 410 cm. As mentioned earlier, two separate cases have been treated:

Case A – has a simple bioshield geometry consisting of only the homogeneous concrete region as given in Ref. 2 (has a 109 x 123 mesh grid).

Case B – has a concrete bioshield containing explicit zones that account for several cooling tubes and structural rebar reinforcements (has a 118 x 123 mesh grid).

The Case B model represents a better model of the actual JPDR configuration (with bioshield data from Ref. 3).

The DORT mesh layouts for the two cases are shown in Figs. 3 and 4, respectively for Cases A and B, where the dark heavy lines represent major material or component boundaries and the two horizontal dark dashed lines identify where the internal boundary sources were saved for subsequent computations above and below Region 2. Notice that the boundary source locations were chosen about 100 cm from the physical model boundaries so that the choice of boundary conditions on the top and bottom surfaces in the central model have little effect on subsequent calculations. Reflected boundary conditions were employed on the left and right and vacuum conditions were imposed on the top and bottom of the Region 2 RZ models.

The material compositions for the various regions highlighted in Fig. 3 for the Case A model were taken directly from Table A.2 in Ref. 2. Identical composition data were used for the Case B model, except for the more explicit modeling in the bioshield region. Table I shows the concrete, steel, and water volume fractions used in the Case B bioshield model (derived from Ref. 3). The Zone 1 - 9 designations in the table map to the nine explicit regions identified in Fig. 4 within the bioshield. These are the single-mesh zones within the heavy lines and they are numbered from left to right, not counting the concrete liner. The 10^{th} zone in Table I is pure concrete and this material occupies all the remaining bioshield regions (with multiple mesh per region). The concrete compositions are identical for Cases A and B, with material densities obtained from Ref. 2.

The material composition data for the various regions and the material IDs from the BUGLE-93 library were used as part of the mixing table within GIP[5] to create a set of 47-group macroscopic cross sections for use within the DORT transport calculations. Although scattering expansions up to 5^{th} order are available within the BUGLE-93 library, only P_3 data were used in these benchmark calculations.

Manually add mesh structure here

Fig. 3. DORT mesh structure for the JPDR Case A model.

Manually add mesh structure here

Fig. 4. DORT mesh structure for the JPDR Case B model.

Table I. Volume fractions for Case B bioshield model.

		Volume Fractions		
Zone #	Description	Concrete	Steel	Water
1	vertical rebar & cooling pipes w/o water*	0.6928	0.1138	0.0000
2	horizontal rebar	0.8482	0.1518	0.0000
3	vertical cooling pipes with water	0.8466	0.0552	0.0982
4	vertical rebar	0.8841	0.1159	0.0000
5	horizontal rebar	0.8482	0.1518	0.0000
6	vertical rebar	0.9337	0.0663	0.0000
7	horizontal rebar	0.9346	0.0654	0.0000
8	horizontal rebar	0.9346	0.0654	0.0000
9	vertical rebar	0.9333	0.0667	0.0000
10	concrete regions	1.0000	0.0000	0.0000

*Since there is no water within the pipes, the volume fractions sum to less than unity.

Because of the size of the computational model, a variable quadrature scheme within DORT was adopted to help cut back on the overall computational time. An S_{16} symmetric quadrature was maintained on both sides of the internal boundary source locations for fine angular detail in these regions. The S_{16} set was also used near the core periphery and radially outward through the cavity to a short distance in the bioshield. These are the zones of most interest in the Region 2 model. In particular, the angular discretization approximation in the cavity region is especially important since axial streaming up and down the voided cavity becomes the dominant source of neutrons to all regions adjacent to the cavity. All remaining areas in the model used a symmetric S_8 quadrature set – including the central core, outer bioshield, and regions well above (top) and below (bottom) the internal boundary source lines. Preliminary calculations with a single S_{16} quadrature throughout the full model verified the validity of the variable quadrature approximation. Therefore, all calculations reported herein used the variable quadrature option within DORT, with about a 20% reduction in run time relative to the full S_{16} case.

The final information necessary to run DORT was the space-energy source distribution within the core region of the JPDR models. Numerical estimates of the spatial source distribution were obtained from Figs. A.2 and A.3 in Ref. 2. A spline fit to the discrete radial and axial profiles produced a continuous distribution and, with this information, the relative source strength associated with the specific mesh spacing utilized in the UMass-Lowell JPDR models was obtained. The RZ spatial source distribution is then simply the product of the radial and axial profiles, S(r,z) = S(r)*S(z).

The source energy spectrum for the 47-group computations was obtained by integrating the Watt fission spectrum over the appropriate 47-group energy grid. Finally, the total source was normalized such that 1 MW of thermal power is generated within the core. Using typical values for the energy per fission (κ = 200 MeV/fiss) and average number of neutrons per fission (ν = 2.5 n/fiss), the source normalization factor in DORT for a power of 1 MW is

$$\mathrm{XNF} = \frac{\nu}{\kappa}\mathrm{P} = \left(\frac{2.5\ \mathrm{n/fiss}}{3.204\times10^{-11}\ \mathrm{W-s/fiss}}\right)\left(10^{6}\ \mathrm{W}\right) = 7.803\times10^{16}\ \mathrm{n/s}$$

Note that the actual power level at any specific time is handled within ACTIV via a simple time-dependent normalization of the absolute flux for the 1 MW power case.

With all the necessary data defined, the DORT calculations were made with a pointwise convergence criterion in the important regions of 0.001. The full space and energy dependent scalar flux data were saved for subsequent use in ACTIV. In addition, some post-processing of the multigroup data – collapsing of the data to three broad groups – was performed for summary presentation of key radial and axial flux profiles. Of particular interest were the profiles in the locations where measured activity data are available.

Figures 5 and 6 show typical radial and axial broad-group flux profiles obtained from the JPDR Region 2 Case B computational model. Group 1 represents fast neutrons above 0.1 MeV, Group 3 is the thermal group with energies below 0.4 eV, and Group 2 covers all energies between these limits. The radial profiles in Fig. 5 are for a height of 360 cm, which corresponds to the location where the measured horizontal distribution of the ^{60}Co activity within the pressure vessel is available. The axial profiles in Fig. 6 are taken at the radial location corresponding to the first mesh point in the concrete bioshield.

Although the profiles in Figs. 5 and 6 behave qualitatively as expected, they also illustrate, quite nicely, the rapid change in neutron spectrum that occurs at various locations throughout the excore regions. The most dramatic example, of course, is the very large attenuation of the thermal flux in the vessel – which has a significant impact on the effective activation cross section versus distance within the vessel. A similar rapid change in the flux spectrum occurs within 20-30 cm of the bioshield, but , in this case, the thermal flux is increasing, rather than decreasing, relative to the epithermal and fast fluxes. These spectral shifts are also seen in the axial direction, although the observed changes are certainly not as severe as in the radial direction.

The impact of these spectral shifts can be illustrated by computing the effective activation cross sections versus position, taking into account the explicit change in the multigroup weight function at each spatial point. A good example is given in Fig. 7

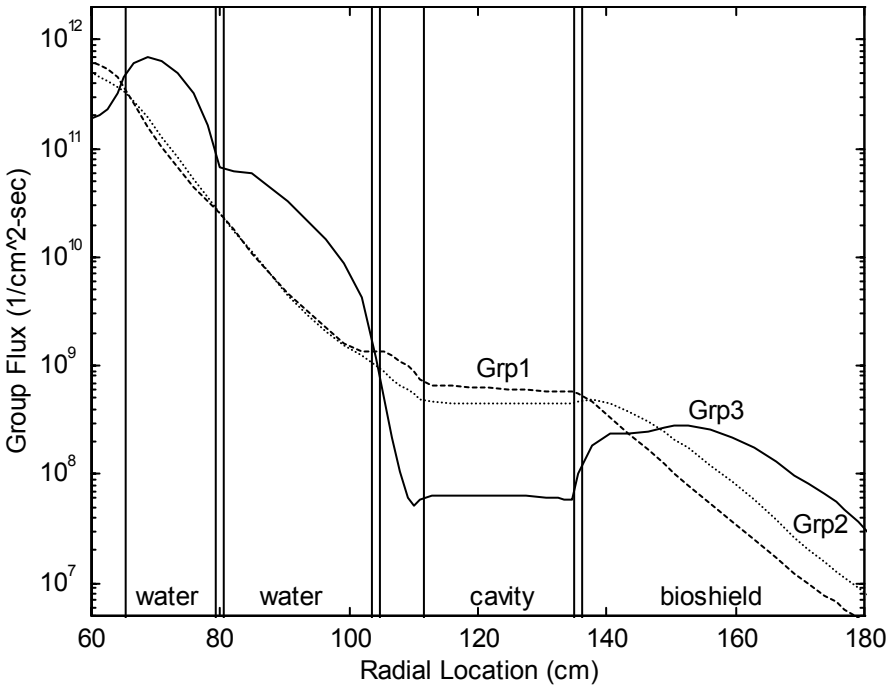

Fig. 5. JPDR broad-group radial flux profiles at H = 360 cm.

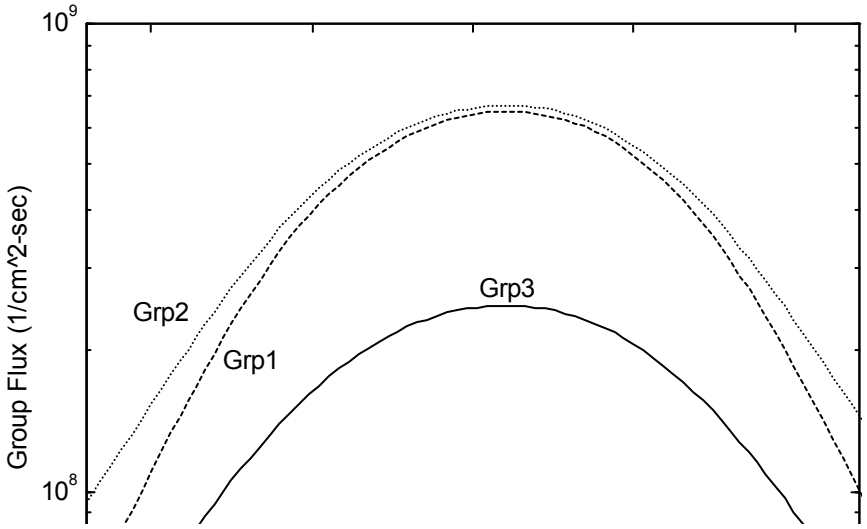

Fig. 6. JPDR broad-group axial flux profiles at inner surface of bioshield.

which shows the effective ^{59}Co n,γ cross section versus radial position at an axial height of 360 cm in the Case B JPDR model. Note that the 1-group average cross section varies by about a factor of 4-5 in the two regions shown in Fig. 7 (pressure vessel and bioshield regions). This phenomenon is certainly significant and it must be treated with reasonable care if reliable activation calculations are desired. Since the ACTIV code models this space-energy coupling in full detail, all the uncertainty related to the use of zone and energy averaged cross sections in the usual zero-dimensional activation analysis is eliminated completely.

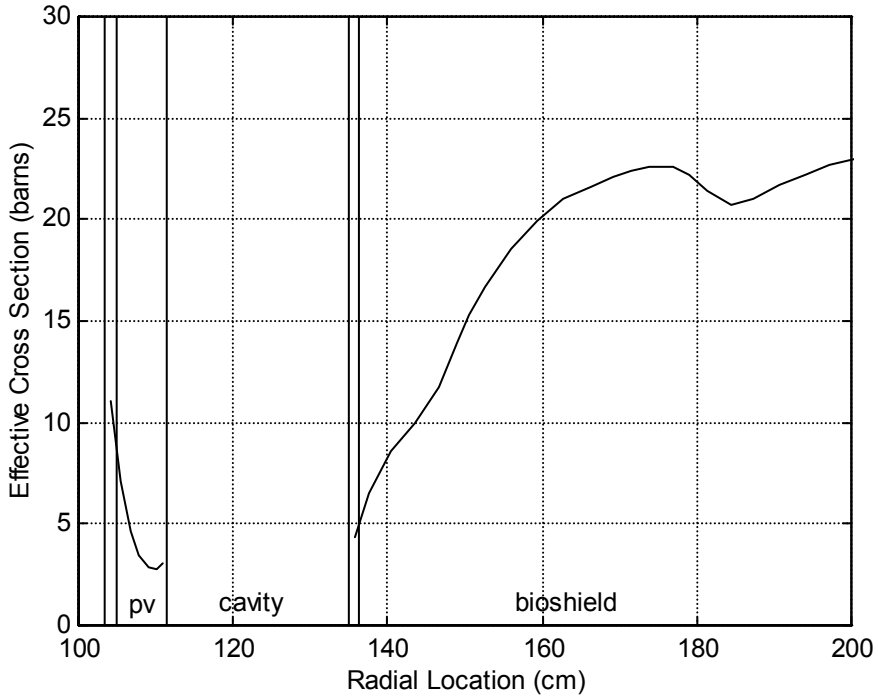

Fig. 7. ^{59}Co 1-group n,γ cross section at H = 360 cm in JPDR.

Activation Analysis Results

Using the 47-group fluxes from the DORT cases and the 47-group activation cross sections in VB6ACTXS.LIB, ACTIV was run using the chain and decay data given in Table II and the initial parent densities given in Table III. Note that the current calculations focus on the activities associated with ^{54}Mn, ^{55}Fe, ^{60}Co, ^{63}Ni, ^{152}Eu, and ^{154}Eu because these were measured as part of the experimental program in the JPDR. The activity of ^{134}Cs was also measured at selected locations within the bioshield, however, its parent isotope, ^{133}Cs, is not available in the current VITAMIN-B6 library. Therefore, the activity associated with ^{134}Cs could not be included in this study.

Table II. Nuclide chain and decay data used in ACTIV.

Parent Isotope	Abundance (a/o)	Daughter Isotope	Halflife (days)	Process
^{54}Fe	5.81	^{54}Mn	3.1215+2	n,p
^{54}Fe	5.81	^{55}Fe	9.9711+2	n,γ
^{59}Co	100	^{60}Co	1.9248+3	n,γ
^{62}Ni	3.59	^{63}Ni	3.6562+4	n,γ
^{151}Eu	47.9	^{152}Eu	4.8680+3	n,γ
^{153}Eu	52.1	^{154}Eu	3.1377+3	n,γ

Table III. Initial parent densities for various activation materials in the JPDR.

Parent Isotope	SUS27 Core Shroud		ASTM-A167 Vessel Clad		ASTM-A302B Pressure Vessel		Bioshield Concrete	
	7.90 g/cc		7.90 g/cc		7.85 g/cc		2.30 g/cc	
	w/o or ppm	atom density	w/o or ppm	atom density	w/o or ppm	atom density	w/o or ppm	atom density
^{54}Fe	70.7*	3.495-3	71.4*	3.530-3	97.4*	4.785-3	1.9*	2.735-5
^{59}Co	1300	1.048-4	1200	9.677-5	200	1.603-5	6.2	1.456-7
^{62}Ni	9.2*	2.675-4	9.8*	2.849-4	0.55*	1.589-5	.0013*	1.100-8
^{151}Eu							0.59	2.575-9
^{153}Eu							0.59	2.801-9

* These entries represent weight percent and the remaining (unstarred) values in this list have units of parts per million (ppm), where both the w/o and ppm values refer to the naturally occurring material (not the specific isotope). Also, the atom densities are in atoms/b-cm.

The abundances and decay data in Table II came directly from the ORIGEN data libraries from SCALE 4.2.[7] The initial parent concentrations in Table III were taken from Table 2 of Ref. 2. These data were then converted to atom densities (atoms/b-cm) for use in ACTIV. For example, if the base information is given in weight percent, one has

$$N_{ij} = \rho_j \times \frac{w_{kj}}{100} \times \left(\frac{a_i}{100} \times \frac{MW_i}{MW_k} \right) \times \frac{.60225}{MW_i}$$

where

N_{ij} = atom density (atoms/b-cm) of isotope i in material j

ρ_j = mass density (g/cm^3) of material j
a_i = atom percent abundance of isotope i in element k
w_{kj} = weight percent of natural element k in material j
MW_i = molecular weight of isotope i (g)
MW_k = molecular weight of isotope k (g)

If parts per million (ppm) is given instead of weight percent (w/o), one simply replaces (w_{kj}/100) with ($ppm_{kj}/10^6$) in the above equation.

The power versus time history for the ACTIV calculation was taken from Fig. A.4 of Ref. 2. There were ten alternating periods of constant power operation and full shutdown, with the last shutdown period lasting 15 years. This latter time interval represents the time from when the reactor was shutdown permanently to when the activation measurements were made. The total simulation time, from initial startup of the JPDR to the measurement time, was 10011.8 days. Thus, all subsequent activation results are reported for this point in time (relative to startup at time zero).

With all this background to establish some specificity to the actual computations that were performed, we can now finally show some of the calculated activities, with a direct comparison to the data measured in the JPDR decommissioning program. The comparisons are broken into two parts:

Radial Profiles

Fig. 8 ^{60}Co activity in pressure vessel at H = 360 cm for Case A
Fig. 9 ^{60}Co activity in pressure vessel at H = 360 cm for Case B
Fig. 10 ^{60}Co activity in bioshield at H = 340 cm for Case A
Fig. 11 ^{60}Co activity in bioshield at H = 340 cm for Case B
Fig. 12 ^{152}Eu activity in bioshield at H = 340 cm for Case B
Fig. 13 ^{154}Eu activity in bioshield at H = 340 cm for Case B

Each figure comparing the calculated and experimental radial activities has two components. The first part shows a plot of the absolute activities, with the circles representing the measured values and the solid line giving the computed values. The second figure in each set displays the behavior of the ratio of the calculated-to-experimental value (C/E value) with the asterisks showing the actual C/E value at each measurement location and the solid line representing a low-order best fit to these individual points. For the pressure vessel (see Figs. 8 and 9), a quadratic fit was used and, in the bioshield (see Figs. 10-13), a simple linear fit was used for all three cases shown (^{60}Co, ^{152}Eu, and ^{154}Eu).

Axial Profiles for Case B

Fig. 14 ^{60}Co activity at inner surface of core shroud and reactor vessel
Fig. 15 ^{55}Fe activity at inner surface of core shroud and reactor vessel

For the axial comparisons, the plots are also grouped in pairs; this time according to specific isotope. In particular, Figs. 14a and 14b look at the absolute ^{60}Co activities at the inner surface of the core shroud and the inner surface of the pressure vessel liner, respectively. Figure 15a and 15b show similar comparisons for the ^{55}Fe activity profiles. Note that, for the axial profiles in the Region 2 model of the JPDR, only a few measured

data points are available. For this reason, only absolute activities are plotted, since there are not enough points to give informative C/E profiles in the axial direction.

The computed numerical data used in these comparisons are also included in tabular form in the Appendix. For completeness, the data in the Appendix include activities for all the radioactive isotopes computed for the JPDR Case B Region 2 model, not just those presented graphically in the figures.

Concerning the plots, one can easily argue that very good results were obtained for all points through the pressure vessel in both Models A and B. For example, Fig. 8b for Case A shows that the C/E values range from a minimum around 0.80 to a maximum near 1.10. The C/E values for the Case B model (see Fig. 9b) have a similar range, varying from about 0.80 to slightly less than unity. The small differences near the outer periphery of the pressure vessel are due to the differences in the bioshield models for Cases A and B, since some of the neutron population in this region of the vessel is due to backscatter from the bioshield.

The good agreement up through the vessel is also apparent in the axial activity profiles given in Figs. 14 and 15, with a maximum error of about $\pm$25% for the worst locations in the shroud and pressure vessel liner. Thus, the overall accuracy of the calculations, up to and including the vessel, is on the order of $\pm$25%. This is a very impressive finding, especially considering the complexity of the calculations required to produce these comparisons. In addition, although not explicitly stated, it is expected that the experimental data and the initial impurity concentrations in the structural materials have uncertainties approaching, or possibly exceeding, the range of C/E values determined within the vessel of the JPDR configuration.

Figures 10-13, however, show that this same level of accuracy is not achieved in the exvessel bioshield region. In fact, the relative error starts out at roughly 50-100% too high, and the error tends to grow with distance into the shield, approaching factors of about 10 and 6, respectively, for Cases A and B at approximately 100 cm into the shield. This behavior is consistent for all the isotopes and the error trend is roughly linear with distance into the concrete region.

Clearly there is a problem in the prediction of the bioshield activities. In fact, it was the large discrepancies in the preliminary results from the Case A model with the simple bioshield geometry that prompted further investigation into the details of the bioshield configuration. The new information from Ref. 3 led to the more detailed Case B bioshield configuration and, as shown in Figs. 10 and 11, the new model did indeed improve the C/E values, both at the surface and at larger distances into the bioshield.

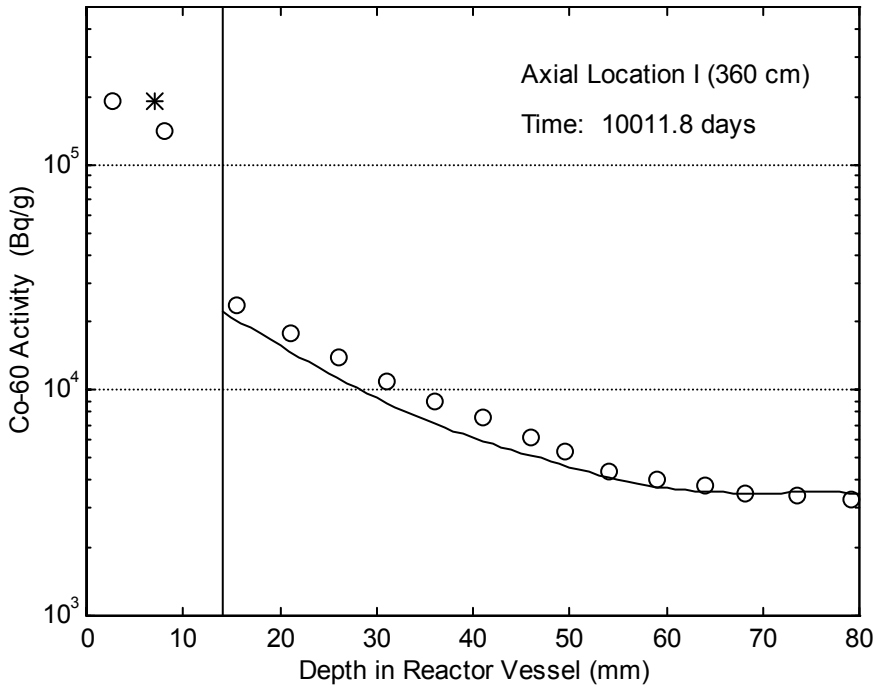

Fig. 8a. Absolute ^{60}Co activity profile within the reactor vessel for Case A.

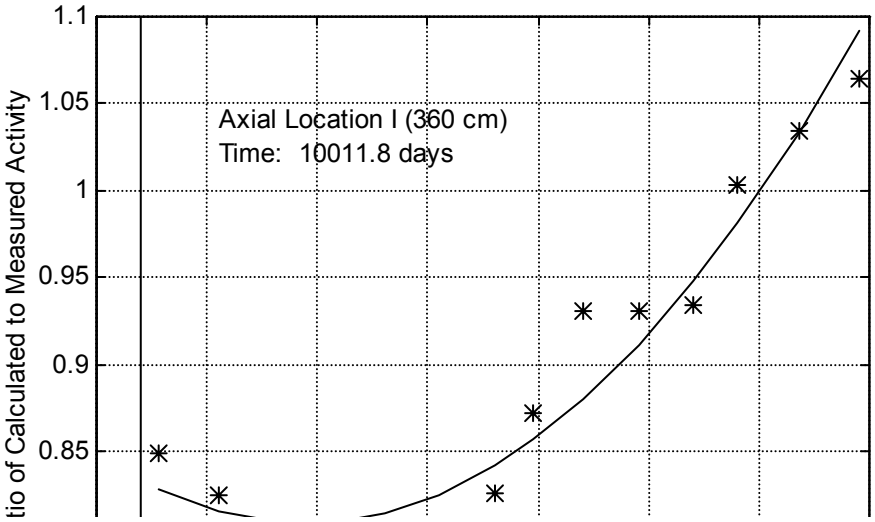

Fig. 8b. C/E profile for the ^{60}Co activity within the reactor vessel for Case A.

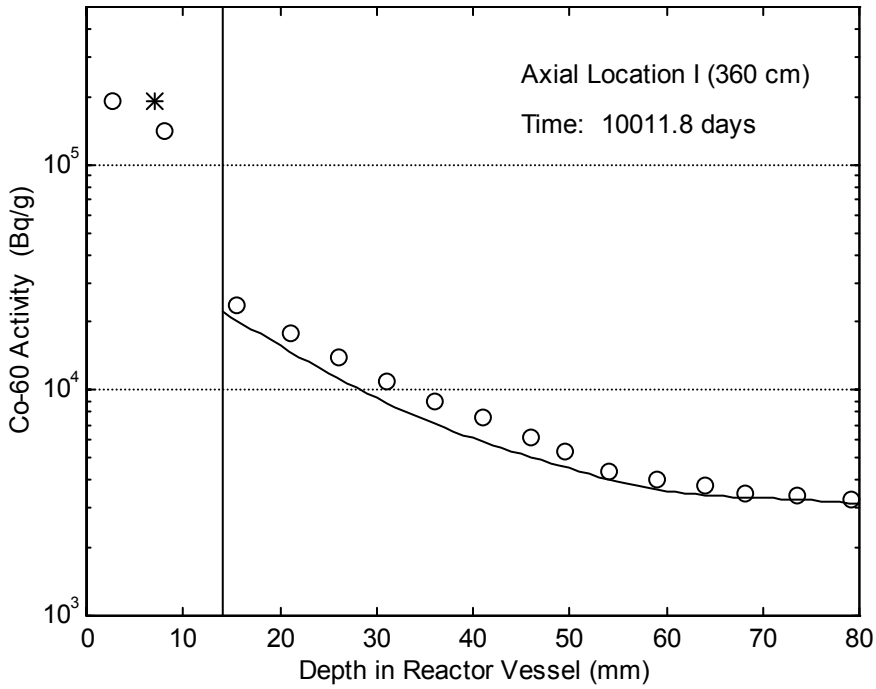

Fig. 9a. Absolute ^{60}Co activity profile within the reactor vessel for Case B.

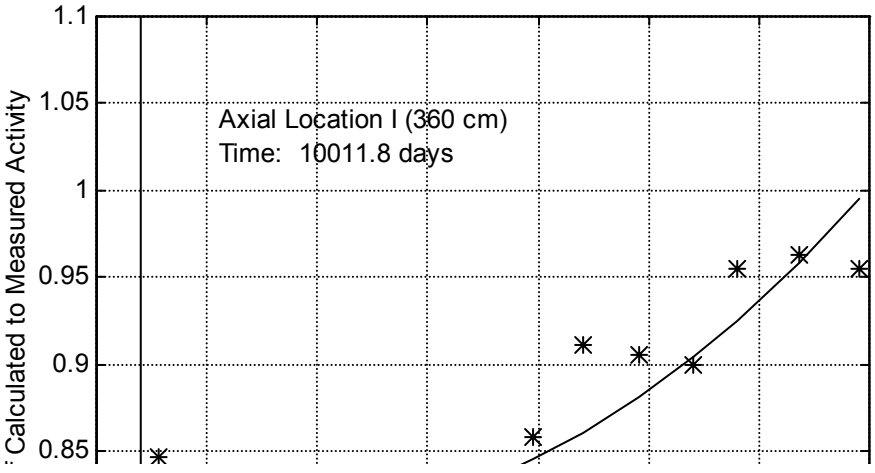

Fig. 9b. C/E profile for the ^{60}Co activity within the reactor vessel for Case B.

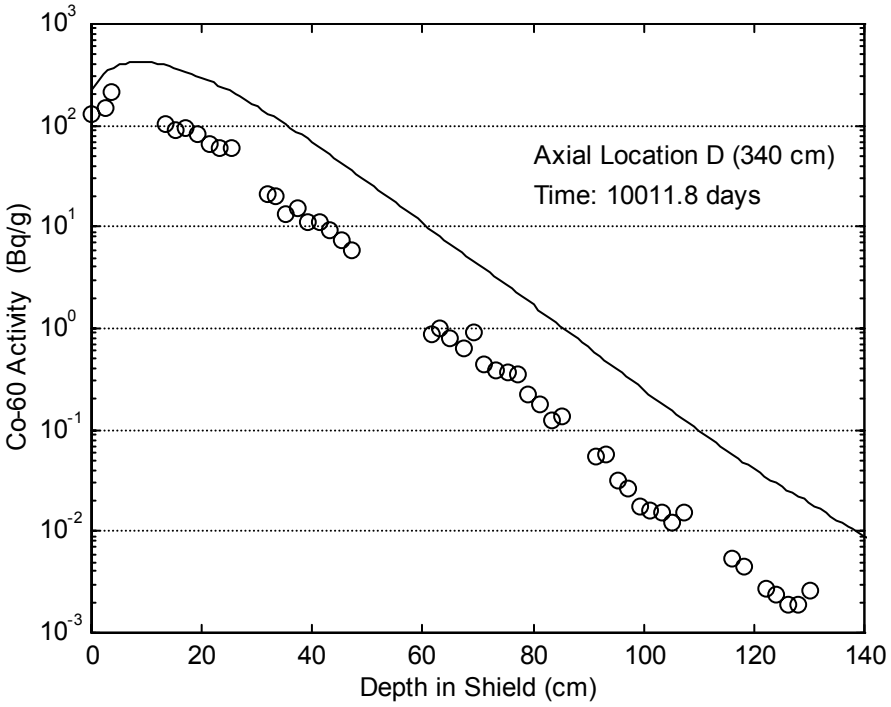

Fig. 10a. Absolute ^{60}Co activity profile within the bioshield for Case A.

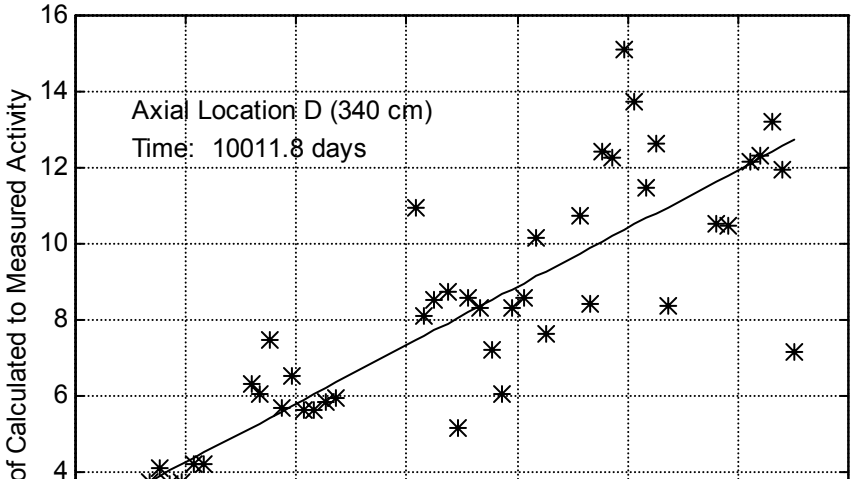

Fig. 10b. C/E profile for the ^{60}Co activity within the bioshield for Case A.

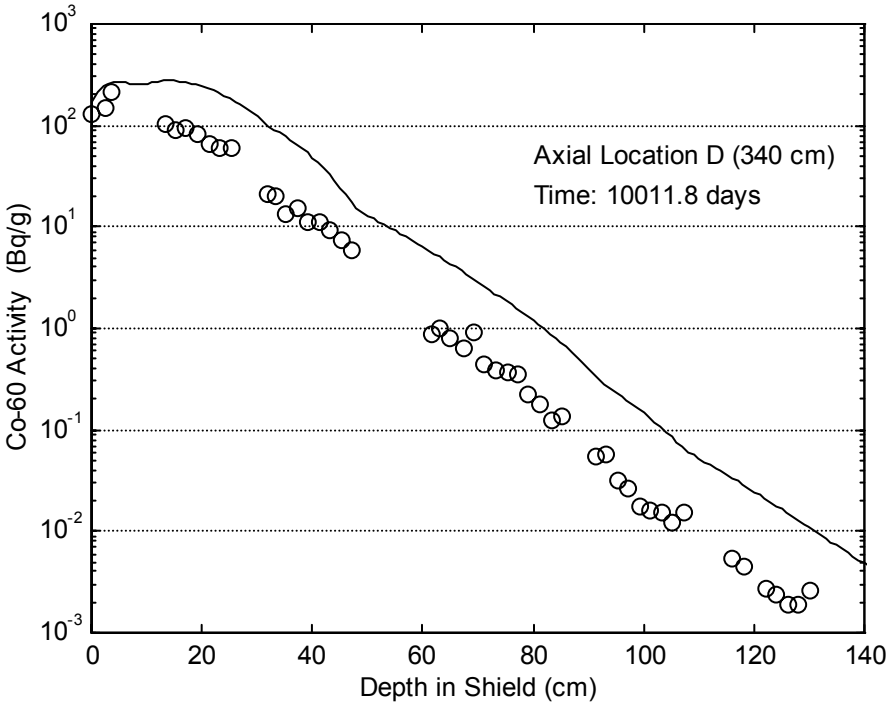

Fig. 11a. Absolute ^{60}Co activity profile within the bioshield for Case B.

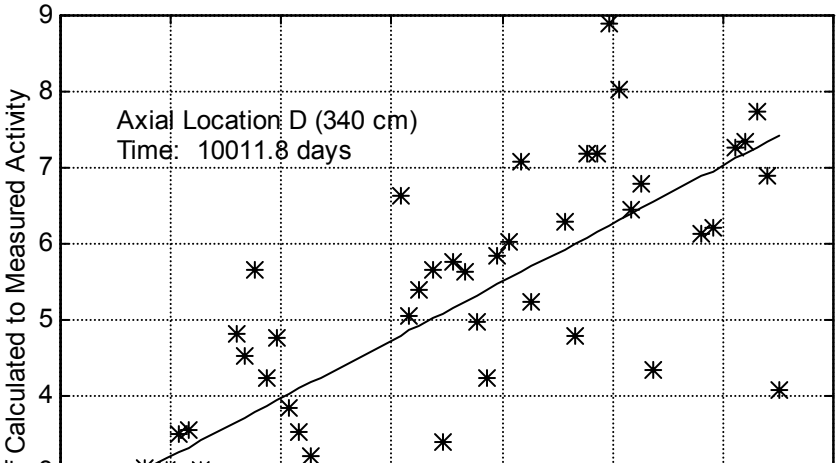

Fig. 11b. C/E profile for the ^{60}Co activity within the bioshield for Case B.

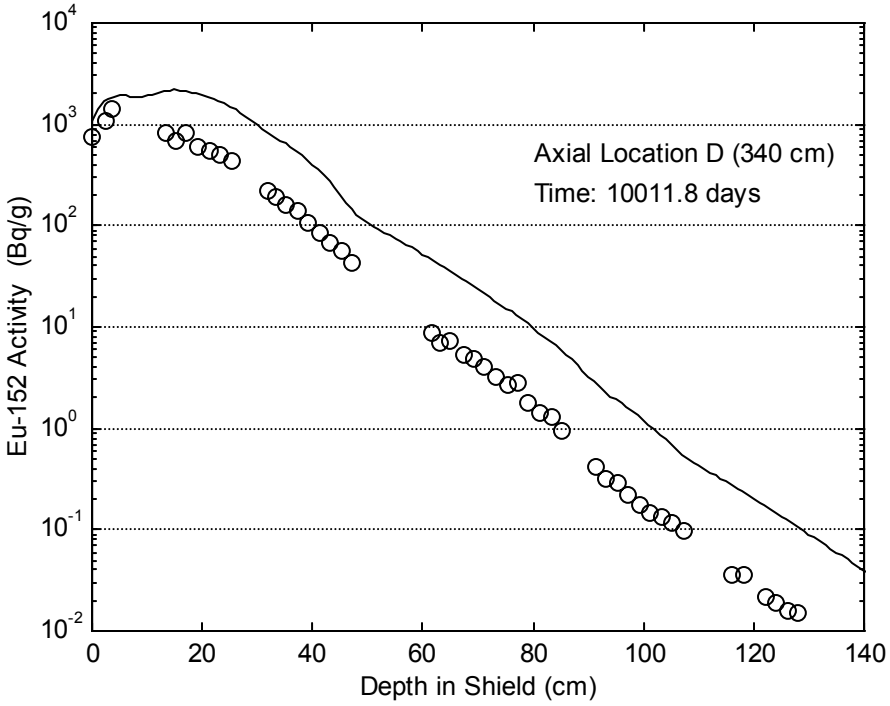

Fig. 12a. Absolute ^{152}Eu activity profile within the bioshield for Case B.

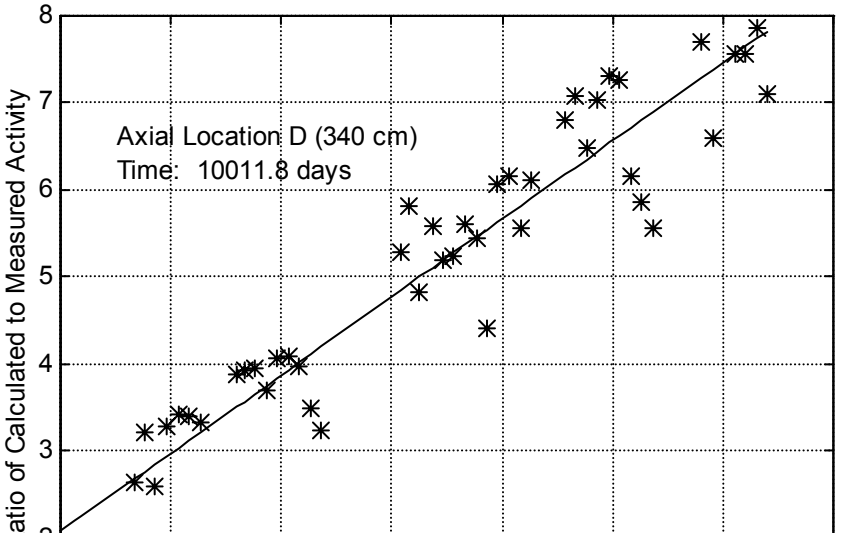

Fig. 12b. C/E profile for the ^{152}Eu activity within the bioshield for Case B.

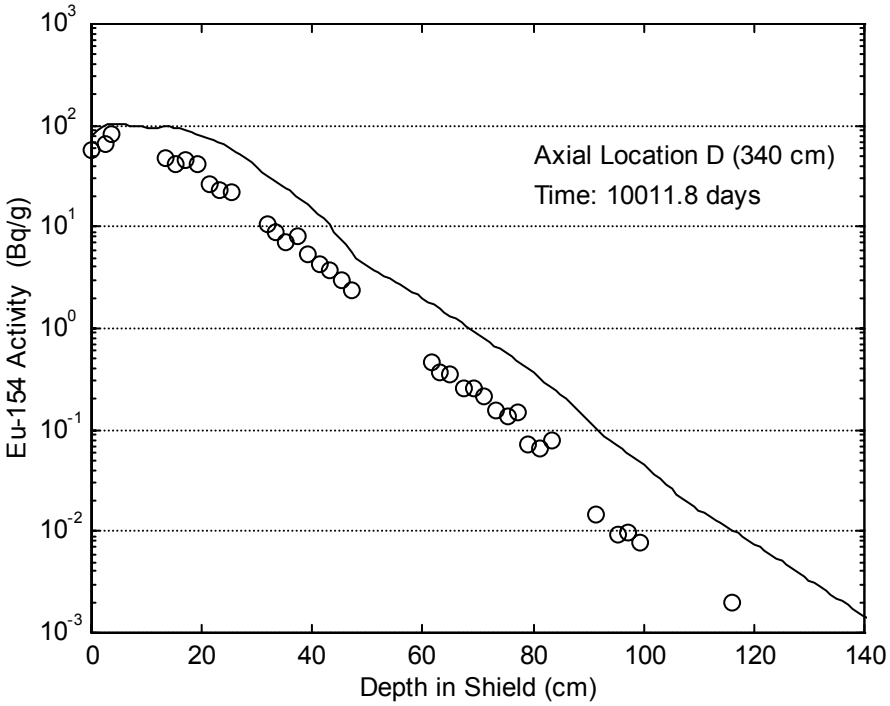

Fig. 13a. Absolute ^{154}Eu activity profile within the bioshield for Case B.

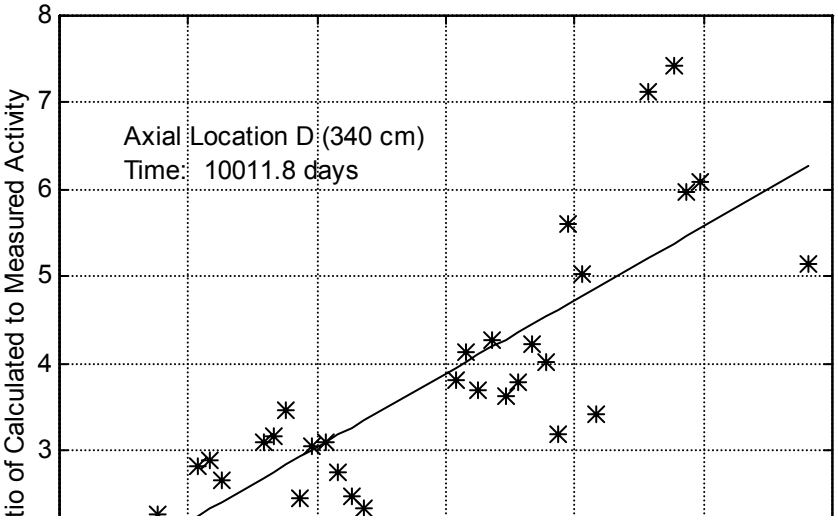

Fig. 13b. C/E profile for the ^{154}Eu activity within the bioshield for Case B.

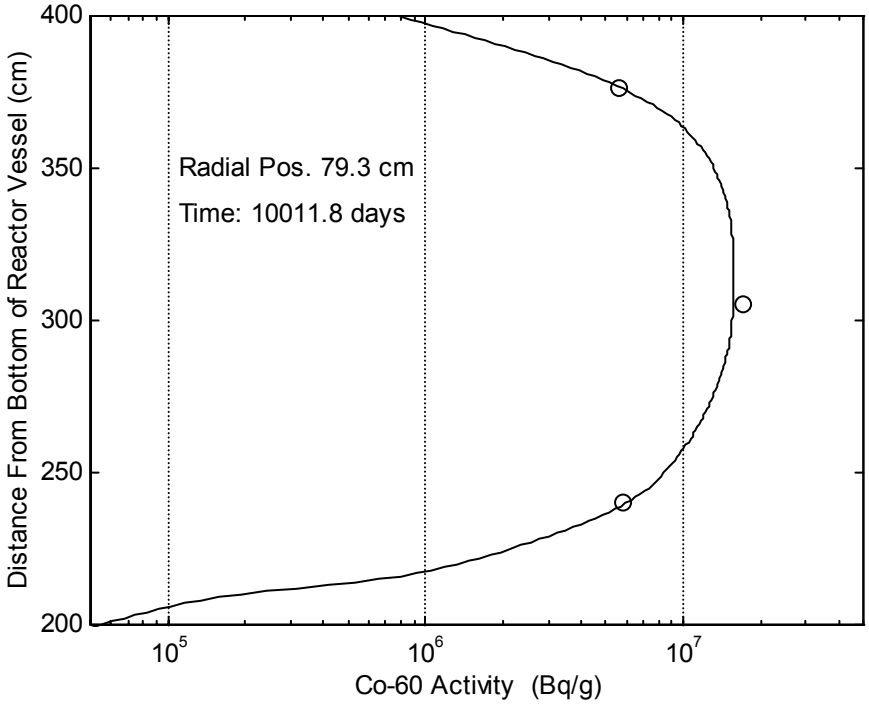

Fig. 14a. Absolute ^{60}Co activity profile along inner surface of shroud for Case B.

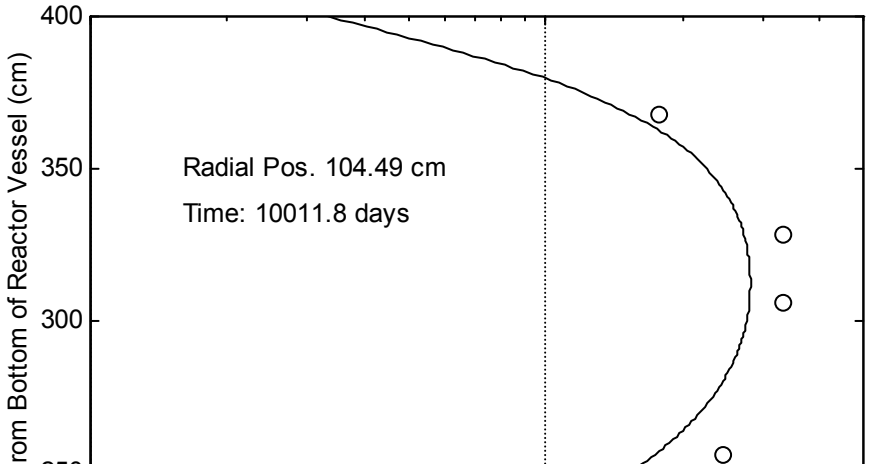

Fig. 14b. Absolute ^{60}Co activity profile along inner surface of vessel for Case B.

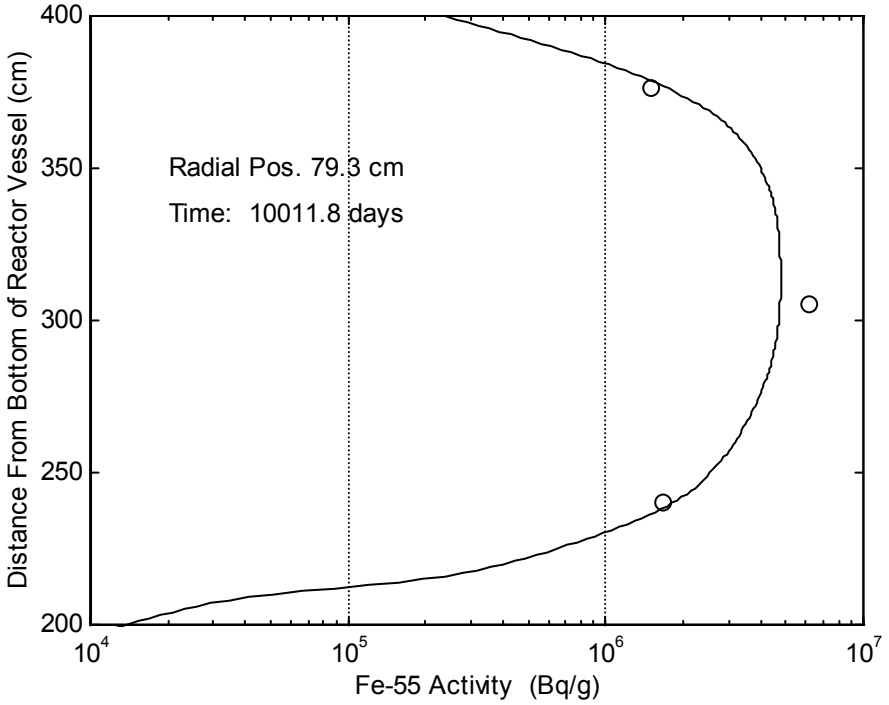

Fig. 15a. Absolute ^{55}Fe activity profile along inner surface of shroud for Case B.

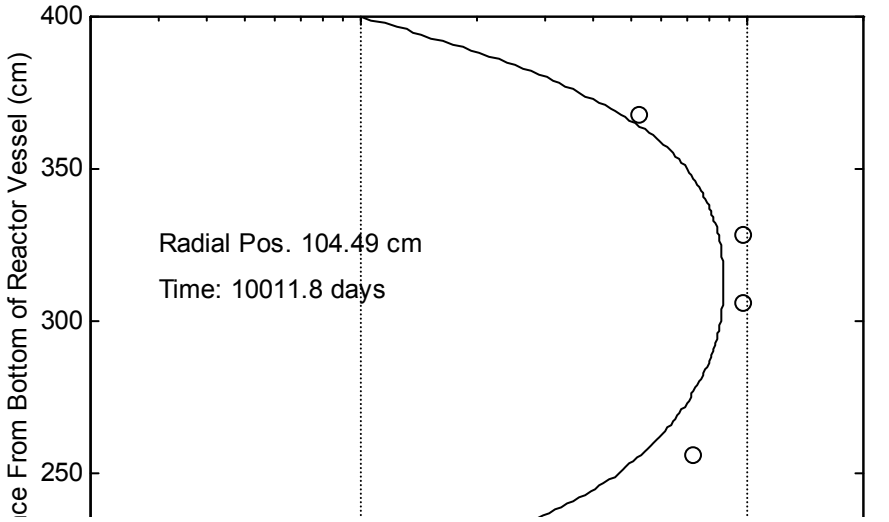

Fig. 15b. Absolute ^{55}Fe activity profile along inner surface of vessel for Case B.

The comparisons given in Figs. 10 and 11 focus on ^{60}Co, but the differences for the Case A and Case B activities were similar for all the isotopes addressed in this benchmark.

However, even with an improved geometric model, the discrepancies in the bioshield are still larger than desired. The root cause of these discrepancies has not been isolated explicitly, although a number of sensitivity studies (quadrature order, mesh spacing, concrete composition, energy resolution, etc.) has identified the relatively poor low-energy resolution in the BUGLE-93 library as a possible culprit. In fact, it is very probable that the 47 group BUGLE-93 library may have been a poor choice for performing this benchmark exercise. Further work is ongoing to address this concern (see below).

Finally, on a positive note, a larger uncertainty with distance into the bioshield, although worrisome from a modeling and analysis viewpoint, is probably not of real concern in practice, since the activity levels are so low anyway. The ^{60}Co activity, for example, is reduced by about 6 orders of magnitude at 100 cm into the shield relative to the magnitude at the inner surface of the pressure vessel. Thus, for disposal and general decommissioning concerns, the activity of the concrete beyond the first 100 cm is negligibly small compared to other components in the system. A factor of 5-10 error in a negligibly small activity may not be of practical concern – but it sure does leave room for some improvements in the data and methods.

Summary/Future Work

This paper summarizes the UMass-Lowell results of a benchmark exercise posed by the IAEA to test data and methods for computing the inventory of several radioactive isotopes that impact decisions concerning the decommissioning of fission reactors. The Japan Power Demonstration Reactor (JPDR) was chosen for this test because of an available data base of measured radial and axial activity profiles for several isotopes and locations in the excore structural regions of the reactor system.

In the UMass-Lowell benchmark tests, the DORT discrete ordinates transport code and the 47-group BUGLE-93 cross section library were used to compute the space and energy distribution of the neutron flux in the regions directly surrounding the core of the JPDR. In addition, a library of activation cross sections with the same group structure as BUGLE-93 was derived from the 199-group VITAMIN-B6 data set. Finally, the ACTIV code, along with the DORT multigroup fluxes and consistent multigroup activation cross sections, was used to compute the time dependent inventory of several isotopes produced via neutron activation over the life of the reactor.

The computed activities from ACTIV, when compared to the measured data from the JPDR decommissioning program, showed very good agreement in all cases for spatial points up to and including the reactor vessel. Calculational errors in these tests were typically less than $\pm$25%. Similar comparisons in the bioshield regions, even with a relatively detailed geometric model, showed much larger differences – typically a factor of 50% or more too high initially, with the error increasing roughly linearly with distance into the bioshield.

The good comparisons that were observed in the pressure vessel regions are very encouraging and they suggest that the basic procedure used for these analyses (DORT, BUGLE-93, ACTIV, and a compatible multigroup activation library) are indeed adequate to the task at hand. These comparisons also serve as an independent validation of the recently developed ACTIV code.

The results in the bioshield, on the other hand, are quite disappointing. However, the consistent behavior that was observed for all the isotopes does suggest that much of the discrepancy is due to inadequate knowledge of the flux magnitude, spectrum, and overall attenuation characteristics, and not due to the activation cross sections and basic methodology. Thus, the search for the root cause of the observed errors should focus on the DORT computation of the space-energy fluxes in the JPDR bioshield.

In addressing this concern, preliminary sensitivity studies have identified the relatively poor thermal energy resolution within the BUGLE-93 library (recall that there are only two groups below 0.4 eV) as a possible source for the majority of the errors observed in the bioshield regions of the JPDR configuration. The relatively hard spectrum in the vessel reduces the importance of thermal activation in this region, but in the concrete bioshield, the much softer spectrum magnifies the need for a good computation of the thermal flux. Previous studies have noted the inadequacy of this particular 47 group structure for computing the thermal fluxes in the excore regions of large PWR systems.[10] Also, as part of the current project, some 1-D fine group calculations for the JPDR model using the XSDRN code[7] with the 199 neutron group VITAMIN-B6 library show significant differences from the thermal flux computed via consistent 47-group 1-D calculations with DORT using BUGLE-93. The full ramification of these differences has not been determined yet, but an ACTIV computation using the 199 group XSDRN fluxes collapsed to 47 groups shows that the new thermal fluxes produce significantly better comparisons with the JPDR experimental data. These studies are not complete, but they do suggest that the two thermal groups in the BUGLE-93 library are not sufficient to adequately represent the rapidly changing thermal flux spectrum in the first 20-30 cm of the JPDR bioshield.

Based on these conclusions, further studies needed to fully complete this benchmark exercise can be grouped into two categories:

1. Completion of the neutron transport and activation calculations for the regions above and below the central axial region that was modeled in the current work.
2. Investigation and resolution of the discrepancies observed in the bioshield region.

The first item, although straightforward, is a major effort simply because of the shear size of the reactor system being modeled. Recall that the full axial dimension of the JPDR is over 12 m, and that the plan is to break the full geometry into three boot-strapped models. Appropriate boundary sources from the centrally located Region 2 model have been saved so that neutron transport calculations, above and below Region 2, can be continued. The completion of these additional calculations will provide activation information in areas far above and below the core region. This should be a good test of our ability to compute neutron transport into these remote regions. At

present, these computations have relatively low priority – at least until the bioshield discrepancies are completely resolved.

The second area for future work is less well defined, since there could be several factors contributing to the discrepancies in the bioshield. It does appear, however, that the poor thermal energy resolution in the BUGLE-93 library is the dominant factor, but further work is needed to prove this theory. What is really needed to test this theory is a new library, similar in all respects to BUGLE-93, but with more thermal energy detail (possibly 7 or 8 thermal groups, instead of only two groups below 0.4 eV). Unfortunately, developing and testing a new multigroup library (say 53 groups) for general neutron and gamma transport analyses and shielding applications, as well as for excore activation computations, is a relatively major undertaking. Even so, we feel strongly that this is the direction to follow. If successful, the space-energy activation analysis methodology utilized in this work could become the definitive tool for performing accurate excore activation studies – studies that could provide the predictive support needed for the planning of safe and economical decommissioning strategies.

References

1. N. Kocherov, “Benchmark on Radioactive Inventory Calculations for Fission Reactor Decommissioning,” letter to potential participants in benchmark exercise (1994).
2. T. Sukegawa, et. al., “ Accuracy Verification for Calculation of Inventory in JPDR Due to Neutron Activation,” International Atomic Energy Agency, INDC(JPN)-164 (1993).
3. Letter from N. Kocherov (IAEA) to J. R. White (UMass-Lowell) dated March 31, 1995 containing detailed drawings from JAERI describing the central part of the JPDR bioshield.
4. J. R. White, et. al., “Maine Yankee Dosimetry Capsule and Pressure Vessel Neutron Fluence Calculations,” **Reactor Dosimetry ASTM STP 1228** (1994).
5. “TORT - A Three Dimensional Discrete Ordinates Transport Code,” Radiation Shielding Information Center Computer Code Collection, CCC-543 (1990). This manual also contains the DORT code and document.
6. D. T. Ingersoll, et al., “Production and Testing of the VITAMIN-B6 Fine-Group and the BUGLE-93 Broad-Group Neutron/Photon Cross-Section Libraries Derived from ENDF/B-VI Nuclear Data,” Oak Ridge National Laboratory, ORNL-6795 (1994).
7. “SCALE 4.2 - Modular Code System for Performing Standardized Computer Analyses for Licensing Evaluation,” Radiation Shielding Information Center Computer Code Collection, CCC-545 (1993).
8. J. R. White, “The DEPTH-CHARGE Static and Time-Dependent Perturbation/ Sensitivity System for Nuclear Reactor Core Analysis, Revision I,” Oak Ridge National Laboratory, ORNL/CSD-78R (1985).
9. D. R. Vondy, et. al., The BOLD VENTURE Computation System for Nuclear Reactor Core Analysis,” Oak Ridge National Laboratory, ORNL-5711 (1981).
10. J. R. White, et. al., “Comparison of the BUGLE-80 and SAILOR Libraries for Coupled Neutron-Gamma Transport Applications,” **Reactor Dosimetry ASTM STP 1228** (1994).